

Comagnetometer probes of dark matter and new physics

W. A. Terrano and M. V. Romalis

Physics Department, Princeton University

Modern comagnetometry is – in absolute energy units – the most sensitive experimental technique for measuring the energy splitting between quantum states, with certain implementations measuring the nuclear spin-up/spin-down splitting at the 10^{-26} eV level. By measuring and subtracting the leading magnetic effects on the spins, comagnetometry can be used to study non-standard-model spin interactions. New physics scenarios that comagnetometers can probe include EDMs, violations of Lorentz invariance, Goldstone bosons from new high-energy symmetries, spin-dependent and CP-violating long-range forces, and axionic dark matter. We describe the many implementations that have been developed and optimized for these applications, and consider the prospects for improvements in the technique. Based purely on existing technology, there is room for several orders of magnitude in further improvement in statistical sensitivity. We also evaluate sources of systematic error and instability that may limit attainable improvements.

1. INTRODUCTION AND HISTORY OF THE FIELD

Following the discovery of nuclear spins in 1933[1] and the demonstration of control over them via their magnetic moments in 1938[2] – accomplishments earning the 1943 Nobel prize for Otto Stern and the 1944 Nobel prize for Isidor Rabi respectively – nuclear magnetic resonance burgeoned as a technique in condensed matter and medical physics, beginning with the experiments of Bloch and Purcell[3, 4] in 1946 for which they shared the 1952 Nobel prize. The first use of nuclear spins for fundamental physics¹ – and with it the development of comagnetometry – took place in 1960 when Hughes[5] and Drever[6] compared the magnetic resonances of ^7Li and a proton at different orientations of the ^7Li quadrupole relative to the galactic center.

A challenge when searching for new physics with spin-dependent couplings is that the magnetic interactions of the spins dwarf the anticipated new physics signals by several orders of magnitude. The simplest nuclear-spin Hamiltonian for a system with total angular momentum \vec{F} is

$$(1) \quad \mathcal{H}_{\text{spin}} = \mathcal{H}_{\text{mag}} + \mathcal{H}_{\text{BSM}} + \dots = \vec{\mu}_N \cdot \vec{B} + \vec{\sigma}_N \cdot \vec{\beta} + \dots$$

with the additional terms depending on the specific comagnetometer implementation. Magnetic interactions \mathcal{H}_{mag} are described by the magnetic moment of the nucleus $\vec{\mu}_N = \mu \vec{F}/F$ and the magnetic field \vec{B} . Beyond-the-Standard-Model interactions \mathcal{H}_{BSM} are described by the spin moment of the nucleus $\vec{\sigma}_N = \vec{F}/F$ and an effective field $\vec{\beta}$ appropriate to the new coupling of interest. For instance, in an electric-dipole-moment search $\vec{\beta} = d_N \vec{E}$ with \vec{E} the applied electric field, and d_N the searched for EDM.

To extract \mathcal{H}_{BSM} from $\mathcal{H}_{\text{spin}}$ the experimentalist typically applies a characteristic time-dependence to $\vec{\beta}(t)$. Even so, the effect of fluctuations in \mathcal{H}_{mag} must be suppressed to eliminate correlations – coincidental or systematic – between the time-dependences of $\vec{\beta}$ and \vec{B} . Comagnetometry achieves this by comparing spins with differing $\vec{\mu}$ or differing $\vec{\beta}$. Other experimental approaches for studying similar types of new physics have been used as well, as summarized in a recent review, for example[7].

Since the era of Hughes and Drever, comagnetometry has improved in absolute energy sensitivity by 12 orders of magnitude. Figure 1 shows the progress in measuring the energy of a nuclear spin pointing due its orientation in absolute space. Comagnetometers built for other purposes[8, 9] have achieved energy sensitivities in the 10^{-26} eV range.

¹Ramsey used bare neutrons for a neutron EDM measurement in 1951 that went unpublished until 1957, when the discovery of parity violation convinced them to publish their negative result.

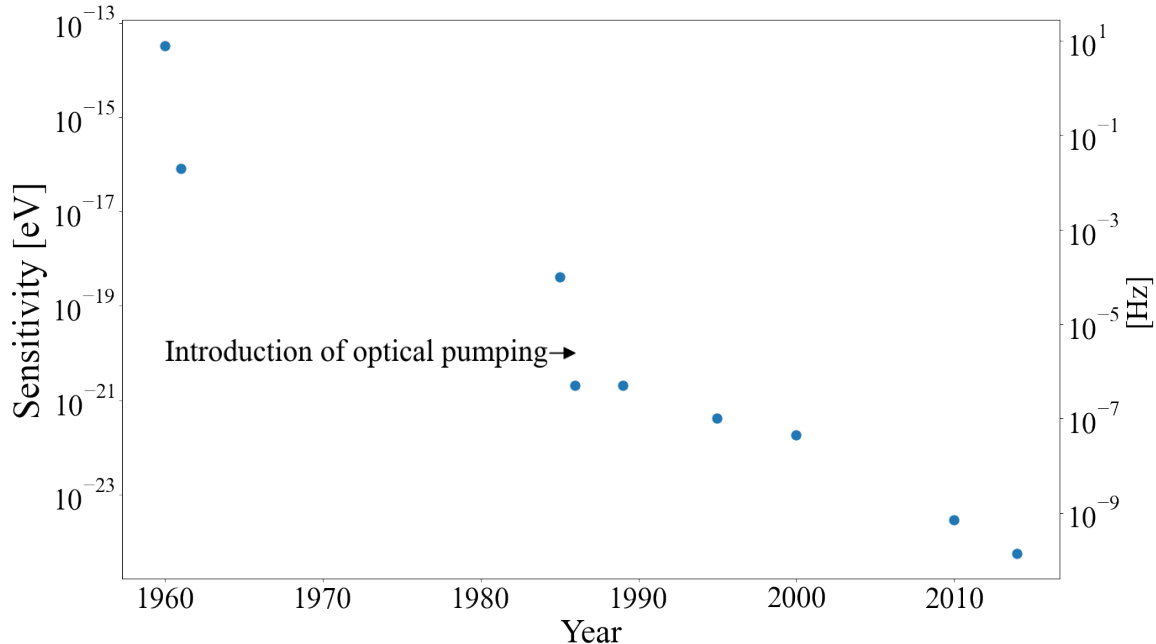


FIGURE 1. The progress in comagnetometer energy sensitivity since Hughes and Drever. These results are for the energy of a spin due to its absolute orientation. The largest improvements came with the ability to create relatively pure ensemble quantum states via optical pumping, in the 1980s, and with the implementation of quantum magnetometers for the read-out systems in the 2000s. References, from top-left to bottom-right: [5, 6, 10–16]

2. COMAGNETOMETRY

A variety of comagnetometer implementations have been developed, with applications to angular-rotation sensing and fundamental physics. This section provides a brief description of comagnetometers used in probes of fundamental physics. This article – and only to limit the scope – focuses on comagnetometers that use at least one nuclear spin. This means important electron-spin comagnetometers such as those used in electron EDM experiments, which compare the energies of various electronic spin states[17–20], and spin pendulums which compare the interactions of electronic spin and electronic orbital angular momentum[21, 22] are left out.

State-of-the-art comagnetometers all use optical pumping – in some fashion – to generate highly nonthermal spin ensembles. Schematically, optical angular momentum is transferred from a laser to an electronic state by optical pumping, and then on to the nucleus. Depending on the transition energies of the atomic states and the wavelengths of available lasers, some nuclear hyper-fine states can be pumped directly while others are polarized via spin-exchange collisions with more easily pumped atoms[23–25].

2.1. General comagnetometer considerations. The main types of nuclear-spin comagnetometers are distinguished by comparison type (energy splitting or quantization axis), spatial distribution (overlapping or not), nuclear spin species of interest, and readout system.

2.1.1. Comparison type: Clock vs quantization axis.

Clock comparisons: The precession frequency f_i of each spin ensemble i is measured, giving its spin-up/spin-down energy splitting $\Delta E_{\text{spin}} = hf_i$. The f_i are then combined in ratios or linear combinations which isolate \mathcal{H}_{BSM} as well as possible from \mathcal{H}_{mag} and other non-BSM contributions

to $\mathcal{H}_{\text{spin}}$. Clock comparisons are mostly limited by state-dependent self-interactions of the spins and by back-action of the read-out system on the nuclei, necessitating precise and repeatable initialization of the ensemble state and quantum decoupling techniques. Specific clock-comparison based comagnetometers are discussed in sections 2.2.1 and 2.2.2 and the references therein.

Quantization-axis comparisons: The quantization axes of two spin ensembles are compared to determine if there is a component of \mathcal{H}_{BSM} acting on one of the ensembles. These systems are largely limited by nanoradian instability in the read-out and polarization systems, which also affect the quantization axes, and by trade-offs between signal size and polarization lifetime. Specific systems based on quantization-axis comparison are discussed in section 2.2.3, and the references therein.

2.1.2. Spatial distribution: overlapped vs separated.

Spatially-overlapped spins: The spin ensembles are contained in a single chamber, so that they nominally sample the same volume and the same \vec{B} . Since the ensembles are in the same chamber they must be different species. Surface effects, gradients in temperature and gradients in polarization decay mean the volume coverage can never be perfectly identical. Sections 2.2.1, 2.2.2, 2.2.3 and references therein discuss spatially-overlapped comagnetometers in more detail.

Spatially-separated spins: The spin ensembles are located in separate chambers. This allows the comparison of spins of the same species, or spin species which require significantly different environmental conditions. Since they are not in the same volume they do not sample the same magnetic field. However, by using several cells drifts in both \vec{B} and gradients of \vec{B} can be canceled. If the same species is used in all chambers, $\vec{\beta}$ must be different in the different chambers. Section 2.2.1 and references therein discuss spatially-separated comagnetometers in more detail.

2.1.3. Choice of Nucleus.

The nucleus must contain an unpaired nucleon, in order to have net spin. All comagnetometers thus far have used isotopes with spin 1/2 or 3/2. The spin 3/2 nuclei have mass and charge quadrupoles allowing them to probe categories of interactions that are inaccessible to spin-1/2 nuclei, although the charge quadrupole couples to electric field gradients and shortens the spin ensemble coherence time. All competitive comagnetometers in recent decades have used either mercury or one of the three noble gases (helium, neon and xenon) that have stable isotopes of spin $\leq 3/2$ in reasonable abundance. Table 1 summarizes the most commonly used nuclei.

Mercury can be pumped and probed directly with UV light, has a high vapor pressure at convenient temperatures and has remarkably long nuclear-spin lifetimes² and high-sensitivity to CP-violation due to its nuclear structure[26]. Noble gases can have much higher densities than Hg vapors at room temperature. However at high densities they can only be hyper-polarized via fairly slow collisional-exchange-polarization techniques. The spin-polarization lifetime must be much longer than the polarization time to achieve highly coherent ensembles. This naturally leads experimental attention to the highly-inert noble gases; gases which form molecules depolarize too rapidly.

2.1.4. Read-out system.

All read-out systems measure the magnetic moments of the nuclei. For mercury, the transitions used to polarize the nuclei can also be used to read-out the nuclear-spin orientation by optical (Faraday) rotation of a linearly-polarized probe beam. Noble gas systems have been built both with optical magnetometers and pick-up loop magnetometers.

Optical magnetometers typically utilize the same alkali atoms as are used to polarize the nuclei, and have the virtue of nearly complete overlap between the magnetic sensor and the nuclear spins. In addition, the effective magnetic field experienced by alkali-metal spins is enhanced due to contact interactions with the nuclear spins. This enhancement ranges from a factor of 5 for helium to ~ 500 for xenon[25, 27]. The tight coupling between the magnetometer and the nuclei leads to significant

²In the hundreds of seconds, corresponding to many collisions

Isotope	Spin	Pumping	Phase
^{199}Hg	1/2	optical	vapor
^{201}Hg	3/2	optical	vapor
^3He	1/2	SEOP/MEOP	gas
^{21}Ne	3/2	SEOP	gas
^{129}Xe	1/2	SEOP	gas
^{131}Xe	3/2	SEOP	gas

TABLE 1. Commonly used nuclei in comagnetometry. SEOP refers to spin-exchange-optical-pumping, wherein nuclear spin polarization is built up via collisions with an atom which can be optically pumped, typically potassium or rubidium. MEOP is metastability-exchange-optical-pumping, wherein a metastable state is optically pumped and then exchanged to the ground state during collisions.

back-action by the magnetometer atoms on the nuclei, which is the main drawback of the approach (along with its sensitivity to optical alignment). Decoupling and stabilizing the read-out is also challenging, since any feedback or control pulses applied to the magnetometer also affect the co-located nuclei as well[28].

External magnetometers significantly reduce these disturbances to the spins – both from back-action and from magnetometer feed-back and decoupling systems. Optimally coupling an external magnetometer to the spins while minimizing magnetometer noise can be challenging technically, however[29].

2.2. Comagnetometer implementations for fundamental physics. In this section we describe the general operating principles of comagnetometers used for fundamental physics. Currently there are three leading implementations with roughly comparable energy resolution: The Hg-EDM comagnetometer (Sec. 2.2.1), the alkali-noble gas self-compensating comagnetometer (Sec. 2.2.3), and the He-Xe-SQUID clock-comparison (Sec. 2.2.2). We also touch on several important implementations that paved the way to modern comagnetometry. New concepts which are under development are mentioned in “Future directions: Novel comagnetometers” (Sec. 4.2). Fundamental physics motivations, signatures and measurements are described in Section 3.

2.2.1. Mercury comagnetometers. The ^{199}Hg - ^{201}Hg comagnetometer, a spatially-overlapping clock comparison, was developed in 1983[30] and was the first comagnetometer to utilize optical pumping and optical readout. The original apparatus was built to search for a dipole-dipole force between electrons and neutrons. Improved versions were used to search for preferred reference frames[11] and spin-gravity interactions[31].

The ^{199}Hg - ^{199}Hg comagnetometer is unique in utilizing a single spin- species, and as such uses spatially separated spin ensembles. The design is completely intertwined with its application in searching for an EDM, and it is discussed in detail in section 3.1 on EDM searches. Since its first implementation in 1987 the sensitivity of this comagnetometer to an EDM has improved from 10^{-26} e-cm to $7 \cdot 10^{-30}$ e-cm [9, 32–36].

Mercury/cesium comagnetometers are spatially-separated clock comparisons of ^{199}Hg nuclei and Cs electrons, and were first built in 1995[13]. This avoids the quadrupolar ^{201}Hg nucleus and has been used to search for preferred frames[13, 37] and for long-range 5th forces[38–40].

2.2.2. Noble-gas/noble-gas clock-comparison. Clock comparisons between pairs of noble gases date back to the 1980s and the development of dual-nuclear-spin-species optical pumping via spin-exchange with rubidium[12, 41], which underpins all implementations. The first version compared ^3He and ^{21}Ne to study local Lorentz invariance[12]. It used a single chamber containing the two gases and alternated between a polarization period and a measurement period, with the measurement using NMR excitation and read-out techniques.

The ^3He - ^{129}Xe maser, a spatially-overlapping clock-comparison, was built in the 1990s[42–44] and used for EDM[45], 5th force[46] and preferred frame[14] searches. The maser consisted of two chambers, one to generate a population inversion via optical pumping of the spins, and the other to provide readout and the positive feedback needed to maintain the masing. The feedback was applied using pickup coils resonant to the two maser frequencies. The atoms diffused between the two chambers via a small tube.

The ^{129}Xe - ^{131}Xe comagnetometer was built as a gyroscope[47] and used to search for new forces[48]. It is a spatially-overlapped clock comparison with rubidium vapor in the same cell as the xenon. Lasers pumped and probed the Rb directly, and the Xe via the Rb-Xe interaction.

The most recent all noble-gas comagnetometers were ^3He - ^{129}Xe - SQUID systems[16, 29, 49–52]. The noble gases were polarized in a separate Rb spin-exchange optical pumping station and then were transferred to an evacuated measurement chamber. The spins were monitored with a SQUID magnetometer that measured the total magnetic field produced by the gas cell. The precession frequencies of the two nuclei were separated and extracted in data analysis, and a \vec{B}_0 invariant frequency computed:

$$(2) \quad \omega_{\text{inv}} = \omega_{\text{Xe}} - \omega_{\text{He}}(\gamma_{\text{Xe}}/\gamma_{\text{He}}),$$

where ω_i and γ_i are the frequency and gyromagnetic ratios of species $i = \text{He}, \text{Xe}$.

This technique is currently limited by the self-interactions of the nuclear spin-ensembles. Significant further improvement could be possible with improved quantum control and decoupling techniques, as discussed in section 4.1.2.

2.2.3. Alkali-metal/noble-gas self-compensating comagnetometer. These comagnetometers compare the spin-quantization axes of colocated spin ensembles, one spin being an alkali-metal vapor and the other a noble gas (specifically K-He and Rb-Ne). They have been built in a variety of configurations and used to search for preferred reference frames and 5th forces. The principles behind these comagnetometers are given in several publications[53, 54]. The spins are polarized in-situ: a laser optically pumps the electronic spins of the alkali-metal, which in turn polarize the noble-gas nuclei via spin-exchange collisions. When the external magnetic field applied along the pump direction matches the magnetic field exerted by the nuclear spins on the alkali spins, the deflection of the quantization axis of the electrons relative to the pump beam is determined by the difference between the non-magnetic interactions of the electronic and nuclear spins. This cancelation of the external magnetic field is only effective at frequencies below the Larmor frequency of the nuclear spins. In that regime the alkali electronic spins experience such a small net magnetic field that broadening due to alkali-alkali spin-exchange collisions is eliminated, and the alkali-spin orientation can be measured very sensitively via the polarization rotation of a linearly polarized probe beam. This read-out consists of measuring the projection of the alkali-spins along the probe beam axis, so mechanical changes in the relative alignment of the pump and probe beams can be an issue. Designs aiming to ameliorate this mechanical sensitivity are under development. Comagnetometers of this type have been used in searches for 5th forces[8, 55, 56] and preferred frames[15, 57], and are well suited to dark matter direct detection[58, 59].

3. FUNDAMENTAL PHYSICS RESULTS

3.1. Electric Dipole Moment Measurements. Searches for intrinsic electric dipole moments are among the most important precision tests of fundamental physics. An intrinsic EDM – which has yet to be observed in any system – must violate T, and therefore CP, symmetry[60]. Searches for nuclear EDMs are motivated by two major outstanding questions in fundamental physics: the strong-CP problem and the baryogenesis question. The strong-CP problem arises from instanton anomalies that generically produce a CP-violating term in the presence of a non-zero quark

mass[61]. This CP-violating term, whose coefficient (θ_{QCD}) is expected to be $\mathcal{O}(1)$, is measured to be less than 10^{-10} . This discrepancy is the strong-CP problem. The baryogenesis question is: how did the universe come to contain more matter than antimatter? Generating a matter/antimatter asymmetry requires a process that simultaneously violates CP-symmetry, violates Baryon number conservation and is out of equilibrium[62]. No such process in the standard model is sufficiently strong, making the identification of additional CP-violation a key part of understanding how the Universe came to be.

EDM measurements with nuclear-spin comagnetometers began in 1984 using ^{129}Xe [63] and shortly thereafter using ^{199}Hg [32], which has greater sensitivity to the strong-CP parameter θ_{QCD} at equal experimental EDM sensitivity. Here we summarize the most recent measurements of the EDM of diamagnetic atoms; the field of EDM measurements is rich, and there are good recent reviews[20, 64].

The ^{225}Ra EDM is more sensitive to fundamental sources of CP violation than most atoms [26, 67]. The EDM of ^{225}Ra was measured for the first time in 2015 using an optical dipole trap[65] and in a follow-up measurement found to be less than $1.4 \cdot 10^{-23} e\text{-cm}$ [66]. Co-magnetometry was not used in these first-generation experiments, but future experiments will use ^{171}Yb atoms held in the same optical trap as a co-magnetometer

The most recent ^{199}Hg search used 4 chambers, each containing a vapor of ^{199}Hg . Different electric fields were applied to the 4 chambers, allowing the experimenters to cancel fluctuations in the magnetic field and its linear and quadratic gradients while maintaining sensitivity to an EDM via appropriate linear combinations of the 4 measured frequencies. The ^{199}Hg nuclei were polarized by optical-pumping, and the precession rate of the nuclei in each chamber was measured by optical rotation of probe a laser. The most recent measurement, the sixth published iteration, reached an EDM sensitivity of $7 \cdot 10^{-30} e\text{-cm}$ [9]³, setting the tightest constraints on θ_{QCD} and several other potential sources of CP-violation[9, 67]. The measurement was limited by a combination of magnetic field gradients and redistribution of the liquid ^{199}Hg droplets.

The most recent ^{129}Xe EDM searches were noble-gas clock-comparisons (Sec. 2.2.2) between ^3He and ^{129}Xe gases[29, 52]. The ^3He atoms should have a negligible EDM due to their small size[68] while the ^{129}Xe atoms could have a sizable EDM, depending on the high-energy origin of the CP-violation[20, 64, 67, 69–71]. An electric field (\vec{E}) was applied to the cell and inverted every few minutes, so the nuclei experienced many \vec{E} states per measurement. The ω_{inv} during each \vec{E} state was extracted, and then ω_{EDM} calculated by weighting by electric field and inverse-variance of ω_{inv} and taking the mean. This technique reached $1.4 \cdot 10^{-27} e\text{-cm}$ and was limited by slow drifts in ω_{inv} : the duration of each \vec{E} -state was chosen to be shorter than the ω_{inv} drifts to eliminate systematics due to the drifts, but this limited the interrogation time of each electric field state. The drifts seemed to originate from interactions between the nuclei, see Sec. 4.1.2 for more detailed discussion.

3.2. Searches for Preferred Frames. Hughes and Drever’s seminal work[5, 6] marked the first of many searches for preferred frames with spins, motivated by a variety of theoretical ideas including non-universal couplings of gravity and electricity&magnetism, Lorentz-violating scenarios and the observation that CPT-violation generates preferred frames that could couple to spin[72–78]. Searches for preferred-frames using nuclei with charge-quadrupole-moments (spin-3/2 and higher) test the Lorentz-invariance of Maxwell’s equations at much greater sensitivity[11, 73, 79, 80] than can be done with photons[81, 82]. Similar experiments have been done looking for anisotropy of maximum attainable velocity for electrons [83–85]), but they also do not reach sensitivities comparable to experiments with nuclei. Since the preferred frame is presumably fixed in the galaxy, the sensitive axis of the experiment must be modulated relative to the galaxy. Most experiments fix

³The first paper[63] set a limit of $1 \cdot 10^{-26} e\text{-cm}$ and pointed out the technique could potentially improve by 4 orders-of-magnitude. The most recent measurements have nearly reached this target.

their sensitive axis in the lab and use the rotation of the Earth to modulate its direction relative to the galaxy. Other experiments use a rotation stage to change the orientation of the sensitive axis[15, 37, 57].

Searches for preferred frames with the alkali/noble gas comagnetometers (Sec. 2.2.3) used a rotary platform to rotate the entire experiment and move the BSM signal to a higher frequency[15, 57]. This type of comagnetometer has great initial sensitivity but has challenges with long-term stability due to its sensitivity to drifts in the optical alignment. The K-He experiment reached a sensitivity of $3 \cdot 10^{-24}$ eV (0.7 nHz) to a preferred spin-orientation, and the Rb-Ne experiment a sensitivity a few times larger for quadrupolar shifts. These experiments were limited by imperfections in the inversion of the sensitive axis. This becomes a systematic issue due to the gyroscopic effect of the rotation of the lab, which produces a frequency shift that depends on the angle of the sensitive axis relative to the Earth rotation axis.

A search for a preferred frame using the ^3He - ^{129}Xe - SQUID system (Sec. 2.2.2) was made using the rotation of the Earth to modulate the orientation of the sensitive axis relative to the Galactic center. This measurement was limited by self-interactions of the nuclei, which caused frequency drifts that the experimenters attempted to model and separate from the sidereal signature of new physics[16, 50]. There is disagreement both about the specific physical origin of these drifts, and how successful they were at disentangling the drifts from the signature of new physics[86–88].

3.3. 5th Force. An ultra-low-mass, weakly interacting boson can generate a weak, macroscopic force. Such particles are widely predicted and, if the particle is a pseudoscalar, would couple to the axial-current Lagrangian $\mathcal{L}_{\text{ax}} = g_{\text{ax}} \bar{\psi} \partial_\mu a \psi \gamma^\mu \gamma^5 \psi$ and mediate a new force coupled to spin. Such particles – variously referred to as axions or axion-like-particles – are produced as the pseudo-Goldstone bosons of new, high-energy symmetries, just as pions are the pseudo-Goldstone bosons produced by chiral symmetry breaking. The coupling of a pseudo-Goldstone boson to standard-model fermions is given by

$$(3) \quad g_{\text{p}} = C_{\text{f}} m_{\text{f}} / f_{\text{a}}$$

where m_{f} is the mass of the fermion, f_{a} is the energy scale of the symmetry breaking and C_{f} is a dimensionless coupling constant expected to be of order one. If the broken symmetry is not exact, like in chiral SU(2), the boson picks up a small mass $m_{\text{a}} = \Lambda^2 / f_{\text{a}}$ where Λ is the explicit symmetry breaking scale. The interaction mediated by the boson is suppressed at distances larger than the Yukawa length of the boson $\lambda = \hbar / (m_{\text{a}} c)$. Searches for new, long-range spin-coupled forces are therefore a general way to search for new hidden symmetries[89].

A pure pseudoscalar mediates a dipole-dipole (spin-spin) interaction:

$$(4) \quad V_{\text{dd}} = \frac{g_{\text{p}}^2 \hbar^2}{16\pi m_1 m_2 c^2 r^3} \left[(\hat{\sigma}_1 \cdot \hat{\sigma}_2) \left(1 + \frac{r}{\lambda} \right) - 3 (\hat{\sigma}_1 \cdot \hat{r}) (\hat{\sigma}_2 \cdot \hat{r}) \left(1 + \frac{r}{\lambda} + \frac{r^2}{3\lambda^2} \right) \right] e^{-r/\lambda}.$$

Here, $\hat{\sigma}_{1,2}$ are the spins of the two particles, $m_{1,2}$ their masses, and \vec{r} the position vector between them. If the boson has a scalar coupling g_{s} in addition, it also mediates a CP-violating $\hat{\sigma} \cdot \hat{r}$ interaction (sometimes called a spin-mass interaction):

$$(5) \quad V_{\text{md}} = \frac{\hbar g_{\text{s}} g_{\text{p}}}{8\pi m_1 c} \left[(\hat{\sigma}_1 \cdot \hat{r}) \left(\frac{1}{r\lambda} + \frac{1}{r^2} \right) \right] e^{-r/\lambda}.$$

In 5th force searches, the comagnetometer serves as the detector and a source of the new force is placed in the vicinity to modify the energies of the comagnetometer spins. In searches for the dipole-dipole interaction (Eq. 4) the source contains polarized spins. In searches for the monopole-dipole interaction (Eq. 5) the source is unpolarized matter. The energy shift from the new force is typically modulated by varying the source distance or polarization.

Spin-mass interactions of nucleons have been studied since the 1960's, when a proton gravitational dipole moment was briefly claimed, before being ruled out[90]. In comagnetometer searches for a new spin-mass force, a mass of large density is moved closer to and further from the comagnetometer, varying the magnitude of the interaction in Eq. 5 through its \vec{r} -dependence. Many spin-mass experiments using comagnetometers have been performed, optimized for various Yukawa ranges[31, 48, 51, 55, 91].

Spin-spin interactions of neutrons were first studied using a ^{199}Hg - ^{201}Hg comagnetometer and the polarized electrons in nearby magnetized material[30]. The neutron-neutron coupling was first studied using the ^3He - ^{129}Xe maser. A chamber filled with high-polarization-density ^3He sourced the potential, and its polarization was inverted at regular intervals to flip the sign of the spin-spin interaction (Eq. 4)[46]. The best current limits come from a similar experiment performed with an alkali-noble gas comagnetometer (K-He) as the detector[8], which improved on the earlier constraint by 3 orders of magnitude to set a limit on an anomalous nuclear spin-spin interaction at 2×10^{-8} of their magnetic interaction.

The exchange of spin-1 bosons can generate a greater variety of potentials than those given in Eqns. 4 and 5, in particular long-range and velocity dependent interactions[92, 93]. Searches for these interactions can be optimized with different source geometries and motions. For many Yukawa lengths, the best source is the spin-polarization of the Earth and its large rotational velocity[39]. Using the Earth as a source requires specialized comagnetometer geometries, for which the mercury/cesium comagnetometer is being optimized.

3.4. Dark Matter. Axions or axion-like-particles are well-motivated extensions to the standard model of particles, as described in section 3.3. In the following, “axion” refers to anything that couples to the axial-current, including all generic pseudo-Goldstone bosons, and “QCD axion” refers to an axion that also couples to the QCD anomaly, and can thereby solve the strong-CP problem. In addition to mediating new forces, axions would be produced in the early universe and make up some or all of the dark matter of the Universe. Axionic dark matter consistent with cosmological observations can have a vast range of masses, roughly from 10^{-22} eV to 10^2 eV in the simplest scenarios. Historically, dark matter axions which also solve the strong-CP problem have attracted the most attention, but many others have been proposed and there is no specific reason that the dark matter particles need to resolve other outstanding problems in particle physics.

The relevant standard model coupling is the pseudo-scalar Lagrangian discussed in section 3.3, but with the dark matter halo of the galaxy as the source. The non-relativistic Hamiltonian is then[94, 95]

$$H_{\text{ax}} \sim g_{\text{p}} a_0 m_{\text{a}} \left(\sum_j \vec{v}_j \cdot \vec{\sigma}_{\psi} \cos \omega_j t \right),$$

where the summation is over modes j of the axion field. The nuclear-spin energy splitting is modulated by (i) the axion oscillation frequencies $\hbar\omega_j = E_j = (m_{\text{a}}c^2 + m_{\text{a}}v_j^2/2)$, (ii) changes in the interference among the modes which occur on the coherence timescale set by the velocity dispersion of the axions $t_c \sim 2\pi/\omega_j(\Delta v/c)^2 \sim 2\pi 10^6/\omega_j$, and (iii) by experimentally controllable changes in the orientation of the fermion spin σ_{ψ} . The magnitude of the signal is proportional to $a_0 m_{\text{a}}$, where a_0 is the amplitude of the axion wave at the time of the measurement. On average, $a_0 m_{\text{a}} = \sqrt{\rho_{\text{DM}}(\hbar c)^3}$ where ρ_{DM} is the local dark matter density.

Axions which solve the strong-CP problem also induce oscillating EDM moments in nuclei[96]; such axions couple directly to gluon fields and so have an unavoidable contribution their mass which puts them out of the frequency range of existing comagnetometers[97]. Going to higher frequencies requires resonant (NMR) techniques or axion-photon searches. It is uncertain precisely which technique will be optimal for which mass ranges, but it seems plausible that the best strategies will be comagnetometer based from 10^{-22} to 10^{-13} eV (10 nHz - 100Hz)[98].

Some dark-matter searches using comagnetometers have been performed[99, 100], although so far with energy resolutions of a few 10^{-19} eV, significantly worse than that of state-of-the-art comagnetometers which reach 10^{-26} eV. An axion search reaching an experimental sensitivity of 10^{-26} eV would be able to probe axion symmetry scales of 10^{11} GeV, assuming the coupling constant C_f defined in Section 3.3 is one. This level is beyond even the most aggressive constraints inferred from stellar cooling, and within an order-of-magnitude or two of the axion symmetry scales currently probed by ADMX[101].

4. FUTURE DIRECTIONS

4.1. Fundamental and practical limitations. State-of-the-art comagnetometers are the most sensitive measurements of the energy difference between two quantum states, of any type, in terms of absolute energy sensitivity. Different implementations are limited by different sources of instability, which are challenging and time consuming to identify and find solutions to – especially when pushing against multiple sources of instability simultaneously. However, these do seem to be practical rather than fundamental limitations, and there is room for significant further improvement in the fundamental sensitivity of these systems. Of course, precision measurements in the real world that are limited by fundamental noise are rare.

4.1.1. Sensitivity and limitations of the ^{199}Hg comagnetometer. The most recent ^{199}Hg measurement reached a total energy sensitivity of 22 pHz ($9 \cdot 10^{-26}$ eV), and resolution of 6.5 nHz from each 240s measurement[9, 102]. This is a factor of 2-3 larger than the signal-to-noise limit, as computed from the photon shot noise. The excess was attributed to a combination of magnetic-field gradients and migration of the ^{199}Hg droplets, which affected the distribution of the polarized nuclei. Making cells which can support high-coherence times is an art, and much effort has gone into increasing the coherence times and working life of the cells. It is unknown if, and by how much, they may be further improved. The spin lifetimes in the best cells were 600-1000 seconds, with a test cell with natural Hg reaching a coherence time of 1000 seconds[102]. If those coherence times could be matched in 4 cells, the integration time could be increased by a factor of $b = 3 \sim 5$ for an equivalent improvement in statistical sensitivity⁴. Significant further improvement could be achieved by slightly increasing the temperature of the cells to obtain higher ^{199}Hg density, provided that does not introduce new sources of leakage current, which can introduce magnetic fields correlated with reversal of the electric field in the cell[9].

4.1.2. Sensitivity and limitations of noble-gas clock comparisons. The intrinsic frequency resolution of a clock-comparison experiment is described by the Cramer-Rao lower bound (CRLB)[50]

$$(6) \quad \sigma_f^2 \geq \frac{12}{(2\pi)^2 (A/\rho)^2 T^3} C$$

where σ_f is the uncertainty in [Hz], A is the signal amplitude, ρ is the (white-noise) amplitude spectral density in $[A/\sqrt{\text{Hz}}]$, T is the observation time in [s] and C is a dimensionless parametrization of the signal decay⁵.

The signal amplitude A (in magnetic field units) can be written as $A = c_f \mu_0 M_n$, where $M_n = \mu_n n P$ is the nuclear magnetization, given by the product of the nuclear magnetic moment μ_n , nucleon density n and nuclear spin polarization P , and c_f is a dimensionless flux coupling factor that describes the magnetic field sensed by the pick-up coil. The frequency uncertainty σ_f can be

⁴Assuming the ratio of light and dark times remains constant. So far laser related systematics have been below the statistical noise, but they are a source of concern.[102]

⁵ $C=1$ for a constant signal, and $C=1.7$ for a signal that decays exponentially for one decay time.

related to the effective magnetic field sensitivity $\sigma_B = 2\pi\sigma_f/\gamma_n$. Combining these equations we obtain

$$\sigma_B^2 = \frac{2\rho^2}{T} \frac{6C}{(c_f\gamma_n\mu_0M_nT)^2}.$$

The first factor $(2\rho^2)/T$ gives the uncertainty in magnetic field measurement for a time T using a magnetometer with field sensitivity ρ . The second factor on the order of $1/(\gamma_n\mu_0M_nT)^2$ gives a dimensionless sensitivity gain factor due to nuclear spin precession that is proportional to the angle of nuclear spin precession in their own magnetization.

A fundamental factor that can limit the sensitivity is spin-projection noise which, for spin-1/2 systems, is given by[103]

$$(\sigma_f^{\text{SN}})^2 = \frac{C_{\text{SN}}}{(2\pi)^2NT_2T}$$

where T_2 is the decay time, N the number of spins and C_{SN} a constant of order 5-10 that depends on the experimental protocol. Unlike alkali-metal magnetometers, nuclear spin magnetometers are usually not limited by spin-projection noise since they contain 10^{19} or more atoms. In the scenarios considered here the projection-noise limit is below the Cramer-Rao lower bound in all cases⁶.

Table 2 shows parameter values from the most recent ³He- ¹²⁹Xe-SQUID measurement, along with some possible improvements. Table 4 gives the specific experimental configurations (geometries, polarizations and pressures) needed for each improvement. The measurement time T_{Meas} in the most recent experiment was chosen such that $T_{\text{Meas}} \times \text{Drift} \approx \sigma_f$. If the drifts were small enough that the measurement time could last the decay time, the Cramer-Rao bound would improve by an order of magnitude. This would require a three orders-of-magnitude reduction in the drifts. The drifts seem to be caused by interactions among the nuclei[88]; we provide more detail on them and how they may be controlled in the discussion around Eq. 7. The first two upgrades in Table 2 are realistic targets for near-term improvements. The last three are long-term targets which are technically challenging, although all technical requirements have been demonstrated in other experimental systems.

In practice it may not be possible to reach best-ever levels on all parameters simultaneously as there can be trade-offs among them. In particular T_{Decay} is sensitive to the environment in many ways. Still, based only on signal-to-noise considerations, the Cramer-Rao bound can be significantly reduced.

In the real-world, precision experiments are typically limited by environmental noise and systematics rather than fundamental limitations. It is not possible to predict whether all instabilities can be controlled well enough to reach the Cramer-Rao bound: we do not even know all the effects that may be important. We outline some likely sources of instability and what it might take to control them.

- *Longitudinal interactions*: The drifts in current experiments are caused by interactions between the nuclei, described by spin-state dependent Hamiltonians

$$(7) \quad \mathcal{H}_i = \sum_j \mu_0\alpha_{ij}\vec{\mu}_i \cdot \vec{\mu}_j$$

where the $\vec{\mu}_{i,j}$ are the magnetic moments of nuclear spin species i, j , and the components of α_{ij} are coupling strengths on the order of 10^{-2} . All components of α_{ij} are generically non-zero and not canceled in the comagnetometer frequency. The $i = j$ terms depend on the cell geometry.

This Hamiltonian produces a spin-up/down energy splitting if there is a non-zero component of either nuclear spin along \vec{B} , and causes a frequency drift as this ‘‘longitudinal’’

⁶The speculative case is within a factor of a few of the projection-noise limit.

System	Cell Mag [fT]	Coupling [geom.]	Readout [fT/ $\sqrt{\text{Hz}}$]	Self Int. [supp.]	T_{Decay} [s]	T_{Int} [s]	CRLB (σ_f) [nHz]
HeXe-2019	1.3×10^6	4.4×10^{-3}	6	1.5×10^{-3}	8000	500	2.7^a
Near-Term Targets: evolutionary progress							
Suppress Int	1.3×10^6	4.4×10^{-3}	6	3×10^{-6}	8000	8000	0.17
Geometry	1.3×10^6	0.22	1	1×10^{-7}	8000	8000	6×10^{-3}
Long-Term Potential: modified protocols needed							
Best Noise	1.3×10^6	0.22	0.1	1×10^{-8}	8000	8000	6×10^{-4}
Long Decay	1.3×10^6	0.22	0.1	3×10^{-9}	18000	18000	1.7×10^{-4}
High Pol ^b	4×10^7	0.22	0.1	4×10^{-12}	18000	18000	6.3×10^{-6}

TABLE 2. Experimental parameters of the 2019 Xe-EDM experiment[29] and possible improvements. Specific configurations needed to reach these levels are given in Table 4 in the appendix. “Cell Mag”: The magnetic field at the surface of the cell for the limiting species. “Coupling”: The ratio of field at the cell to field through the pick-up loop, which depends on the geometry of the system. “Readout”: The noise in the read-out sensor. This is often dominated by the magnetic noise of the local environment. “Self Int.”: The factor by which the self-interaction Hamiltonian (Eq. 7) must be suppressed, by cancelling terms against each other, preparing the system with very small longitudinal component or decoupling that Hamiltonian. “ T_{Decay} ”: The decay time constant of the transverse amplitude^c. “ T_{Int} ” Measurement time for a single frequency extraction. Taken to be T_{Decay} unless comagnetometer instabilities require shorter durations. “CRLB”: The theoretical best resolution of the experiment, computed for a single T_{Decay} time.

^aThe experimentally measured uncertainty was 3 nHz.

^bGenerating high polarizations of both species simultaneously would require separate pumping cells or advancements in dual-species hybrid pumping, as the optimal pumping conditions for high Xe density and high He density are quite different.

^c $A(t) = A_0 e^{-t/T_{\text{Decay}}}$

component of the polarization decays away[88, 104]. The drift can be suppressed by precise state initialization to ensure there is no longitudinal polarization, decoupling sequences[105], and specially chosen cell geometries[88, 104]. The suppression required can scale faster than the improvement in signal-to-noise ratio in some cases⁷. The improvements outlined in “Near-Term Targets” of Table 2 require suppressing self-interactions by $\mathcal{O}(10^4)$ compared to current experiments. Achieving the “Long-Term Potential” would require significantly greater control over the self-interacting portion of the Hamiltonian, especially if the cell magnetizations are increased.

- *Earth rotation effects*: The nuclei precess in the non-inertial frame of the rotating Earth so they pick-up an apparent frequency shift of $f_{\oplus} \sim 10 \mu\text{Hz}$ for a horizontal magnetic field at mid-latitudes[49]. This shift depends on the angle between the magnetic field and the

⁷Consider improving some aspect of the experiment by a multiplicative factor of b . How much would longitudinal interactions need to be suppressed in order to take full advantage? If the improvement is in the noise (or in signal, if achieved through better spin-SQUID coupling), the longitudinal interactions must be suppressed by $1/b$ to maintain the same integration time. If the increase is in the number of spins – through higher pressures or polarization fraction or both – the longitudinal interactions must be suppressed by $1/b^2$, as the higher polarization increases both the output signal and the internal magnetizations that source the longitudinal self-interactions. If the increase is in T_{Decay} , the longitudinal interactions must be suppressed by $1/b^{3/2}$ to take full advantage of the longer potential integration time. If T_{Int} increases relative to T_{Decay} the required suppression scales as $1/b^{5/2}$ (in the $T_{\text{Int}} \ll T_{\text{Decay}}$ limit) since a larger fraction of the longitudinal magnetization decays during the integration time

Earth’s rotation axis, so anything that changes that angle also changes ω_{int} . Some specific potential issues include: tilts or twists of the apparatus from loading of the Earth’s surface in the vicinity; changes in the background magnetic field; and changes in the orientation of the Earth’s rotational axis. Secular changes in the Earth’s rotation period correspond 0.1pHz changes in ω_{inv} as the Earth’s rotation period itself changes. These slow changes in Earth’s rotation can be monitored and removed easily by stellar observations[106, 107]. Changes in the orientation of the Earth’s rotation axis are known from very long baseline interferometry and observed in ring-laser gyroscopes. In a typical experimental configuration (mid-latitude & horizontal holding field) these changes would contribute daily fluctuations of ~ 0.5 pHz[108]. If the holding field is aligned with the Earth’s rotation axis[31] these are suppressed to tolerable levels (Table 5).

- *Gyroscopic coupling to lab motions*: Slow tilts of the lab due to tidal, atmospheric and local loading can produce a rotation around the sensitive axis of the system, which would be picked up by the same gyroscopic coupling that produces the Earth rotation effect described above. Commercial tilt-meters have a sensitivity around $7 \text{ nrad}/\sqrt{\text{Hz}}$ [109], a few times the resolution needed to monitor and subtract this coupling in the most sensitive scenarios. The success of ring-laser gyroscopes which are sensitive to twists demonstrates that – when care is taken and the apparatus affixed to the bedrock – laboratory twists can be suppressed to around these levels[108].
- *Transverse self-interactions*: Since the cell is not spherical, there will be through-space Ramsey-Bloch-Siegert shifts of the nuclei on each other[16] caused by the magnetic field of the rotating (transverse) component of the nuclear polarization. The signal sizes in the HeXe-2019 system should cause a transverse-magnetization-dependent frequency shift of ~ 500 pHz and scale quadratically with magnetization[88]. Since the rotating amplitudes are measured during data-taking this effect should be possible to account for metrologically.

4.1.3. *Sensitivity and limitations of alkali-noble gas self-compensating comagnetometers*. Alkali-noble gas comagnetometers face three major sources of noise, and the limiting source depends on the frequency and the measurement of interest: at low-frequency, fluctuations in the beam alignment; at high-frequency, the breakdown of the magnetic-field compensation; in the middle, probe beam noise. Experiments which require mechanical motion of the comagnetometer or source masses are often limited by beam alignment across the middle frequencies as well.

The most sensitive comagnetometer ever operated was a K-³He co-magnetometer used to search for spin-spin 5th forces, which reached an integrated sensitivity of 20 pHz (7×10^{-26} eV), with a noise level of 21 nHz/ $\sqrt{\text{Hz}}$ at the signal frequency of 0.3 Hz. This experiment was limited by laser intensity fluctuations at a factor of two above the shot noise limit, and within a factor of 5 of the best-ever alkali-metal magnetometer sensitivity[110].

Beam alignment and magnetic field noise both improve at higher frequencies, so a system with larger magnetization which can operate at higher-frequencies could be more sensitive. The effect of mechanical motion can be reduced with pulsed operation of the pump laser followed by measurements of the transient response of the coupled spin system. Unlike nuclear spin precession magnetometers, the self-compensating magnetometer measures the twist on the nuclei at static equilibrium and so does not have the gain factor due to measuring the precession frequency given by $\gamma\mu_0 M_n T$. Thus its sensitivity is limited by the best available sensitivity of the alkali-metal magnetometer.

4.2. **Novel comagnetometer implementations**. New ideas in comagnetometry are constantly being investigated, aiming for reduced sensitivity to various sources of systematic error. Here we give a brief description of some recent efforts, which explore several interesting avenues.

- $^3\text{He} - ^{129}\text{Xe}/^{21}\text{Ne}$ *with Rb readout*[28, 104, 111]: This system suppresses the longitudinal interactions that limit other noble-gas comagnetometers by using the same volume for pumping and probing, permitting greater refinement and repeatability of the state initialization at the beginning of the probe time. It also increases the signal due to the contact interaction between Rb and nuclear spins. The read-out of the spin precession is done via the Rb in the cell, meaning the back-action of the Rb on the nuclei must be decoupled. This is done using RF-pulses to rapidly invert the Rb orientation so it has no net longitudinal polarization. These pulses also invert the Rb relative to the magnetic field, suppressing spin-exchange relaxation even at the higher magnetic fields needed for noble gas precession measurements. The decoupling pulses themselves produce a species dependent frequency shift that is much smaller than that of the Rb which they decouple but still much larger than the target sensitivity. This requires further decoupling, or operating in the dark with no pulses. Interactions between Rb and ^{21}Ne are ~ 15 times smaller than between Rb and ^{129}Xe , allowing longer spin-precession times and smaller Rb back-action, at the cost of dealing with ^{21}Ne quadrupolar effects. Current data shows the ^{21}Ne quadrupolar frequency splitting is smaller than the ^{21}Ne linewidth, even with decay times of several thousand seconds.
- *Transversely pumped* $^{129}\text{Xe} - ^{131}\text{Xe}$ [112–114]: This system suppresses the longitudinal interactions that limit other noble-gas comagnetometers by pumping the nuclei transversely to the holding field. To pump the Rb perpendicular to the holding field, the magnetic “holding” field is made up of pulses, with each pulse flipping the Rb by 2π . To generate a net Rb polarization along the xenon as the xenon rotate, either the laser polarization was reversed at the xenon frequencies, or the magnetic holding field was modulated so the xenon precess slower when aligned with the beam and faster when anti-aligned. This pump/probe geometry also allows feedback to reduce the build up of longitudinal polarization.
- Dual Xe isotope spin maser[115]: This approach uses a Rb magnetometer to apply positive feedback so the nuclear spins precess indefinitely with continuous optical pumping. Compared to earlier work on spin masers [28,13], this approach can be operated at a lower bias field because it does not rely on inductive detection of spin precession with a pick-up coil. Even though the spins precess indefinitely due to the positive feedback, the sensitivity of spin masers is still given by the Cramer-Rao bound with T equal to the spin coherence time. At longer times the feedback system introduces a random frequency walk due to coupling of the detection noise.
- *Comolecular comagnetometer*[100, 116]: This system compares the ^{13}C and ^1H of liquid state $^{13}\text{CH}_3\text{CN}$ molecules to improve the spatial overlap between the comagnetometer spin-ensembles. These experiments used the classic NMR technique of polarizing the nuclei in a large magnetic field. The lack of hyper-polarization means the energy resolution of the first iteration was around $100\ \mu\text{Hz}$ with 30 days of integration time. There is hope that hyper-polarization may be applied to this system[100].
- *Comagnetometer networks*: Searches for transient anomolous fields are motivated by astrophysical models predicting things such as domain walls, axion vortices or self-gravitating axion clusters. More generally, they are a good way to look for the unexpected[117]. Identifying transients with a single comagnetometer is essentially impossible, as it would be indistinguishable from an experimental glitch. A network of comagnetometers looking for correlated glitches across the globe, however, has a chance of observing such a transient[118].

4.3. Potential Physics Reach. Real physics experiments are limited by systematics, so projections of physics reach are inherently speculative. However, to give an idea of what could be done, Table 3 shows rough sensitivities to the axion-decay-constant and ^{129}Xe EDM if the experimental targets outlined in Table 2 are reached, and control of systematics keeps pace. The “Near-term”

scenario corresponds to line 3 of Table 2 and involves canceling drifts and optimizing the experimental geometry. “Optimistic” scenario corresponds to line 5 of Table 2, and requires matching the best readout noise yet achieved in such a system, as well as the longest published polarization lifetimes. “Speculative” scenario matches the highest spin-polarizations ever achieved – which have not yet been demonstrated in dual-species systems – along with much greater control over internal interactions, which is required because of the higher magnetizations. It may also be possible to improve the readout noise of the system even further, which could be a more profitable approach, although just as speculative.

Experimental progress	Integrated energy resolution [eV (Hz)]	Dark-matter-axion scale F_a/C_n [GeV]	Xe EDM [e-cm]
Near-Term	1×10^{-27} (2.5×10^{-13})	9.6×10^{11}	2.9×10^{-30}
Optimistic	4×10^{-29} (9.4×10^{-15})	2.6×10^{13}	1.1×10^{-31}
Speculative	1.4×10^{-30} (3.4×10^{-16})	7.1×10^{14}	4×10^{-33}

TABLE 3. Physics reach of a ^3He - ^{129}Xe - SQUID system under conservative, optimistic and speculative scenarios, assuming 100 days of measurement. “Integrated Energy Resolution”: The uncertainty on $\hbar\omega_{\text{inv}}$. “Dark-matter-axion scale”: Defined in equation 3, F_a is the symmetry-breaking scale of the axion and C_n is a dimensionless coupling constant to nucleons, assumed to be order one. These limits apply specifically to axions with oscillation frequency below the repetition rate of the experiment, around 10^{-19} eV. “Xe EDM [e-cm]”: The EDM measurements assume 25-33 kV voltage difference across the cell (5 kV/cm electric fields) with 5 high voltage states per decay time. Leakage current effects are largely canceled by the comagnetometer, with measurements constraining an effect of $\leq 1.77 \mu\text{Hz}/\mu\text{A}$. This implies conservative estimates of the maximum allowable leakage currents to be 3.9×10^4 , 110 and 40 fA respectively. The most recent ^{199}Hg measurements measured steady-state leakage currents of 40 fA.

The sensitivities outlined in Table 3 are ambitious, and will require significant advances in the understanding of and control over instabilities in this type of comagnetometer. They are, however, consistent with existing signal-to-noise ratios, which are outstanding thanks to decades of work.

Enticingly, based on these estimates a comagnetometer could come within nearly an order-of-magnitude of some heretofore almost unimaginable targets: axion dark matter produced by symmetry-breaking at the Grand Unification scale of 10^{16} GeV, and the standard-model prediction for the ^{129}Xe EDM of 5×10^{-35} e-cm[20]. If all goes well on the comagnetometry side, and another order-of-magnitude beyond Table 3 is to be achieved, the next technological break-throughs – whether in low-noise magnetic shielding, two-stage readout or elsewhere – may be driven by these fundamental physics motivations.

Acknowledgements: This work was made possible by Princeton University and the Simons Foundation.

APPENDIX A. PHYSICAL PARAMETERS OF POTENTIAL UPGRADES

System	Dimensions [cm]			Xenon		Helium	
	Cell	Pickup	Cell-SQUID	P	pol	P	pol
	Diam.	Diam.	Z	[bar]	[]	[bar]	[]
HeXe-2019	2.0	0.24	2.9	0.14	0.12	0.65	0.004
Near-Term Targets: evolutionary progress							
Suppress Int	2.0	0.24	2.9	0.14	0.12	0.65	0.004
Geometry	5.0	1.4	4.1	0.14	0.12	0.65	0.004
Long-Term Potential: modified protocols needed							
Best Noise	6.7	5.0	4.7	0.14	0.12	0.65	0.004
Long Decay	6.7	5.0	4.7	0.14	0.12	0.65	0.004
High Pol	6.7	5.0	4.7	1.0	0.5	1.1	0.06

TABLE 4. Experimental parameters of the 2019 Xe-EDM experiment[29] and possible future improvements. All parameters have been demonstrated, albeit not necessarily in a comagnetometer system. “Cell-SQUID” is the distance from the center of the cell to the center of the SQUID pickup loop. “P” and “pol” are the pressure and polarization fraction of each noble gas species.

APPENDIX B. REQUIREMENTS ON STABILITY AND MONITORING

Progression	Typical B0			Polar B0		
	Earth Axis [fraction of]	B \perp [fT]	B0 Tilt [μ rad]	Earth Axis [fraction of]	B \perp [fT]	B0 Tilt [μ rad]
Near-Term	0.4	3×10^3	1	220	1×10^7	5×10^3
Optimistic	1.5×10^{-2}	78	2.6×10^{-2}	8	3×10^5	1.5×10^2
Speculative	5.4×10^{-4}	2.7	1×10^{-3}	0.3	1×10^4	5

TABLE 5. Stability requirements on environmental parameters so that associated frequency shifts from changes in the gyroscopic pickup of Earth’s rotation remain below the statistical sensitivity. “Typical B0” are the requirements for a convenient mid-latitude, horizontally aligned magnetic field. “Polar B0” are the requirements if the magnetic field is aligned with the Earth’s rotation axis to within 100μ rad. “Earth Axis” is the changing orientation of the rotation axis of the earth. This is unavoidable and must be subtracted from the measured frequencies based on other observations and geophysical models. This column gives the maximum allowable fractional error in the model of the polar motion at the experiment site. “B \perp ” gives the requirement on how well known the transverse fields at the cell must be known, per measurement point and assuming a 2μ T holding field. “B0 Tilt” gives the requirement on how well tilts along the B0 axis must be known.

REFERENCES

- [1] I. Estermann, R. Frisch, and O. Stern, “Magnetic moment of the proton,” *Nature* **132**, 169–170 (1933).
- [2] I. I. Rabi, J. R. Zacharias, S. Millman, and P. Kusch, “A new method of measuring nuclear magnetic moment,” *Phys. Rev.* **53**, 318–318 (1938).
- [3] F. Bloch, W. W. Hansen, and M. Packard, “The nuclear induction experiment,” *Phys. Rev.* **70**, 474–485 (1946).
- [4] E. M. Purcell, R. V. Pound, and N. Bloembergen, “Nuclear magnetic resonance absorption in hydrogen gas,” *Phys. Rev.* **70**, 986–987 (1946).
- [5] V. W. Hughes, H. G. Robinson, and V. Beltran-Lopez, “Upper limit for the anisotropy of inertial mass from nuclear resonance experiments,” *Phys. Rev. Lett.* **4**, 342–344 (1960).
- [6] R. W. P. Drever, “A search for anisotropy of inertial mass using a free precession technique,” *The Philosophical Magazine: A Journal of Theoretical Experimental and Applied Physics* **6**, 683–687 (1961), <https://doi.org/10.1080/14786436108244418> .
- [7] M. S. Safronova, D. Budker, D. DeMille, D. F. J. Kimball, A. Derevianko, and C. W. Clark, “Search for new physics with atoms and molecules,” *Rev. Mod. Phys.* **90**, 025008 (2018).
- [8] G. Vasilakis, J. M. Brown, T. W. Kornack, and M. V. Romalis, “Limits on New Long Range Nuclear Spin-Dependent Forces Set with a K-He3 Comagnetometer,” *Physical Review Letters* **103**, 261801 (2009), [arXiv:0809.4700 \[physics.atom-ph\]](https://arxiv.org/abs/0809.4700) .
- [9] B. Graner, Y. Chen, E. G. Lindahl, and B. R. Heckel, “Reduced limit on the permanent electric dipole moment of ^{199}Hg ,” *Phys. Rev. Lett.* **116**, 161601 (2016).
- [10] J. D. Prestage, J. J. Bollinger, W. M. Itano, and D. J. Wineland, “Limits for spatial anisotropy by use of nuclear-spin-polarized $^9\text{Be}^+$ ions,” *Phys. Rev. Lett.* **54**, 2387–2390 (1985).
- [11] S. K. Lamoreaux, J. P. Jacobs, B. R. Heckel, F. J. Raab, and E. N. Fortson, “New limits on spatial anisotropy from optically-pumped sup201hg and ^{199}Hg ,” *Phys. Rev. Lett.* **57**, 3125–3128 (1986).
- [12] T. E. Chupp, R. J. Hoare, R. A. Loveman, E. R. Oteiza, J. M. Richardson, M. E. Wagshul, and A. K. Thompson, “Results of a new test of local lorentz invariance: A search for mass anisotropy in ^{21}Ne ,” *Phys. Rev. Lett.* **63**, 1541–1545 (1989).
- [13] C. J. Berglund, L. R. Hunter, D. Krause, Jr., E. O. Prigge, M. S. Ronfeldt, and S. K. Lamoreaux, “New limits on local lorentz invariance from hg and cs magnetometers,” *Phys. Rev. Lett.* **75**, 1879–1882 (1995).
- [14] D. Bear, R. E. Stoner, R. L. Walsworth, V. A. Kostelecký, and C. D. Lane, “Limit on lorentz and cpt violation of the neutron using a two-species noble-gas maser,” *Phys. Rev. Lett.* **85**, 5038–5041 (2000).
- [15] J. M. Brown, S. J. Smullin, T. W. Kornack, and M. V. Romalis, “New Limit on Lorentz- and CPT-Violating Neutron Spin Interactions,” *Physical Review Letters* **105**, 151604 (2010), [arXiv:1006.5425 \[physics.atom-ph\]](https://arxiv.org/abs/1006.5425) .
- [16] F. Allmendinger, W. Heil, S. Karpuk, W. Kilian, A. Scharth, U. Schmidt, A. Schnabel, Y. Sobolev, and K. Tullney, “New limit on lorentz-invariance- and cpt-violating neutron spin interactions using a free-spin-precession ^3He - ^{129}Xe comagnetometer,” *Phys. Rev. Lett.* **112**, 110801 (2014).
- [17] J. Baron, W. C. Campbell, D. DeMille, J. M. Doyle, G. Gabrielse, Y. V. Gurevich, P. W. Hess, N. R. Hutzler, E. Kirilov, I. Kozyryev, B. R. O’Leary, C. D. Panda, M. F. Parsons, E. S. Petrik, B. Spaun, A. C. Vutha, and A. D. West, “Order of magnitude smaller limit on the electric dipole moment of the electron,” *Science* **343**, 269–272 (2014), <http://science.sciencemag.org/content/343/6168/269.full.pdf> .
- [18] W. B. Cairncross, D. N. Gresh, M. Grau, K. C. Cossel, T. S. Roussy, Y. Ni, Y. Zhou, J. Ye, and E. A. Cornell, “Precision measurement of the electron’s electric dipole moment using

- trapped molecular ions,” *Phys. Rev. Lett.* **119**, 153001 (2017).
- [19] ACME Collaboration, V. Andreev, D. G. Ang, D. DeMille, J. M. Doyle, G. Gabrielse, J. Haefner, N. R. Hutzler, Z. Lasner, C. Meisenhelder, B. R. O’Leary, C. D. Panda, A. D. West, E. P. West, and X. Wu, “Improved limit on the electric dipole moment of the electron,” *Nature* **562**, 355–360 (2018).
- [20] T. E. Chupp, P. Fierlinger, M. J. Ramsey-Musolf, and J. T. Singh, “Electric dipole moments of atoms, molecules, nuclei, and particles,” *Rev. Mod. Phys.* **91**, 015001 (2019).
- [21] B. R. Heckel, E. G. Adelberger, C. E. Cramer, T. S. Cook, S. Schlamminger, and U. Schmidt, “Preferred-frame and CP-violation tests with polarized electrons,” *Phys. Rev. D* **78**, 092006 (2008), [arXiv:0808.2673 \[hep-ex\]](#) .
- [22] h. Terrano, E. G. Adelberger, J. G. Lee, and B. R. Heckel, “Short-Range, Spin-Dependent Interactions of Electrons: A Probe for Exotic Pseudo-Goldstone Bosons,” *Physical Review Letters* **115**, 201801 (2015), [arXiv:1508.02463 \[hep-ex\]](#) .
- [23] H. G. Dehmelt, “Modulation of a light beam by precessing absorbing atoms,” *Phys. Rev.* **105**, 1924–1925 (1957).
- [24] A. L. Bloom, “Principles of operation of the rubidium vapormagnetometer,” *Appl. Opt.* **1**, 61–68 (1962).
- [25] T. G. Walker and W. Happer, “Spin-exchange optical pumping of noble-gas nuclei,” *Rev. Mod. Phys.* **69**, 629–642 (1997).
- [26] J. Engel, M. J. Ramsey-Musolf, and U. van Kolck, “Electric dipole moments of nucleons, nuclei, and atoms: The standard model and beyond,” *Progress in Particle and Nuclear Physics* **71**, 21–74 (2013), fundamental Symmetries in the Era of the LHC.
- [27] S. R. Schaefer, G. D. Cates, T.-R. Chien, D. Gonatas, W. Happer, and T. G. Walker, “Frequency shifts of the magnetic-resonance spectrum of mixtures of nuclear spin-polarized noble gases and vapors of spin-polarized alkali-metal atoms,” *Phys. Rev. A* **39**, 5613–5623 (1989).
- [28] M. E. Limes, D. Sheng, and M. V. Romalis, “ ^3He – ^{129}Xe comagnetometry using ^{87}Rb detection and decoupling,” *Phys. Rev. Lett.* **120**, 033401 (2018).
- [29] N. Sachdeva and I. Fan, “New limit on the permanent electric dipole moment of ^{129}Xe using ^3He comagnetometry and squid detection,” **123**, 143003 (2019).
- [30] E. B. Aleksandrov, A. A. Ansel’m, Y. V. Pavlov, and R. M. Umarkhodzhaev, “A restriction on the existence of a new type of fundamental interaction (the “arion” long-range interaction) in an experiment on spin precession of mercury nuclei,” *Sov. Phys. JETP* **58**, 1103 (1983).
- [31] B. J. Venema, P. K. Majumder, S. K. Lamoreaux, B. R. Heckel, and E. N. Fortson, “Search for a coupling of the earth’s gravitational field to nuclear spins in atomic mercury,” *Phys. Rev. Lett.* **68**, 135–138 (1992).
- [32] S. K. Lamoreaux, J. P. Jacobs, B. R. Heckel, F. J. Raab, and N. Fortson, “New constraints on time-reversal asymmetry from a search for a permanent electric dipole moment of ^{199}Hg ,” *Phys. Rev. Lett.* **59**, 2275–2278 (1987).
- [33] J. P. Jacobs, W. M. Klipstein, S. K. Lamoreaux, B. R. Heckel, and E. N. Fortson, “Testing time-reversal symmetry using ^{199}Hg ,” *Phys. Rev. Lett.* **71**, 3782–3785 (1993).
- [34] J. P. Jacobs, W. M. Klipstein, S. K. Lamoreaux, B. R. Heckel, and E. N. Fortson, “Limit on the electric-dipole moment of ^{199}Hg using synchronous optical pumping,” *Phys. Rev. A* **52**, 3521–3540 (1995).
- [35] M. V. Romalis, W. C. Griffith, J. P. Jacobs, and E. N. Fortson, “New limit on the permanent electric dipole moment of ^{199}Hg ,” *Phys. Rev. Lett.* **86**, 2505–2508 (2001).
- [36] W. C. Griffith, M. D. Swallows, T. H. Loftus, M. V. Romalis, B. R. Heckel, and E. N. Fortson, “Improved limit on the permanent electric dipole moment of ^{199}Hg ,” *Phys. Rev. Lett.* **102**, 101601 (2009).

- [37] S. K. Peck, D. K. Kim, D. Stein, D. Orbaker, A. Foss, M. T. Hummon, and L. R. Hunter, “Limits on local lorentz invariance in mercury and cesium,” *Phys. Rev. A* **86**, 012109 (2012).
- [38] A. N. Youdin, D. Krause, Jr., K. Jagannathan, L. R. Hunter, and S. K. Lamoreaux, “Limits on spin-mass couplings within the axion window,” *Phys. Rev. Lett.* **77**, 2170–2173 (1996).
- [39] L. Hunter, J. Gordon, S. Peck, D. Ang, and J.-F. Lin, “Using the earth as a polarized electron source to search for long-range spin-spin interactions,” *Science* **339**, 928–932 (2013), <https://science.sciencemag.org/content/339/6122/928.full.pdf>.
- [40] L. R. Hunter and D. G. Ang, “Using geoelectrons to search for velocity-dependent spin-spin interactions,” *Phys. Rev. Lett.* **112**, 091803 (2014).
- [41] T. E. Chupp, E. R. Oteiza, J. M. Richardson, and T. R. White, “Precision frequency measurements with polarized ^3He , ^{21}Ne , and ^{129}Xe atoms,” *Phys. Rev. A* **38**, 3998–4003 (1988).
- [42] T. E. Chupp, R. J. Hoare, R. L. Walsworth, and B. Wu, “Spin-exchange-pumped ^3He and ^{129}Xe zeeman masers,” *Phys. Rev. Lett.* **72**, 2363–2366 (1994).
- [43] R. E. Stoner, M. A. Rosenberry, J. T. Wright, T. E. Chupp, E. R. Oteiza, and R. L. Walsworth, “Demonstration of a two species noble gas maser,” *Phys. Rev. Lett.* **77**, 3971–3974 (1996).
- [44] D. Bear, T. E. Chupp, K. Cooper, S. DeDeo, M. Rosenberry, R. E. Stoner, and R. L. Walsworth, “Improved frequency stability of the dual-noble-gas maser,” *Phys. Rev. A* **57**, 5006–5008 (1998).
- [45] M. A. Rosenberry and T. E. Chupp, “Atomic electric dipole moment measurement using spin exchange pumped masers of ^{129}Xe and ^3He ,” *Phys. Rev. Lett.* **86**, 22–25 (2001).
- [46] A. G. Glenday, C. E. Cramer, D. F. Phillips, and R. L. Walsworth, “Limits on anomalous spin-spin couplings between neutrons,” *Phys. Rev. Lett.* **101**, 261801 (2008).
- [47] T. G. Walker, “Fundamentals of spin-exchange optical pumping,” *Journal of Physics: Conference Series* **294**, 012001 (2011).
- [48] M. Bulatowicz, R. Griffith, M. Larsen, J. Mirijanian, C. B. Fu, E. Smith, W. M. Snow, H. Yan, and T. G. Walker, “Laboratory search for a long-range t -odd, p -odd interaction from axionlike particles using dual-species nuclear magnetic resonance with polarized ^{129}Xe and ^{131}Xe gas,” *Phys. Rev. Lett.* **111**, 102001 (2013).
- [49] C. Gemmel, W. Heil, S. Karpuk, K. Lenz, C. Ludwig, Y. Sobolev, K. Tullney, M. Burghoff, W. Kilian, S. Knappe-Grüneberg, W. Müller, A. Schnabel, F. Seifert, L. Trahms, and S. Baeßler, “Ultra-sensitive magnetometry based on free precession of nuclear spins,” *The European Physical Journal D* **57**, 303–320 (2010).
- [50] C. Gemmel, W. Heil, S. Karpuk, K. Lenz, Y. Sobolev, K. Tullney, M. Burghoff, W. Kilian, S. Knappe-Grüneberg, W. Müller, A. Schnabel, F. Seifert, L. Trahms, and U. Schmidt, “Limit on lorentz and cpt violation of the bound neutron using a free precession $^3\text{He}/^{129}\text{Xe}$ comagnetometer,” *Phys. Rev. D* **82**, 111901 (2010).
- [51] K. Tullney, F. Allmendinger, M. Burghoff, W. Heil, S. Karpuk, W. Kilian, S. Knappe-Grüneberg, W. Müller, U. Schmidt, A. Schnabel, F. Seifert, Y. Sobolev, and L. Trahms, “Constraints on Spin-Dependent Short-Range Interaction between Nucleons,” *Physical Review Letters* **111**, 100801 (2013), [arXiv:1303.6612 \[hep-ex\]](https://arxiv.org/abs/1303.6612).
- [52] F. Allmendinger, I. Engin, W. Heil, S. Karpuk, H.-J. Krause, B. Niederländer, A. Offenhäuser, M. Repetto, U. Schmidt, and S. Zimmer, “Measurement of the permanent electric dipole moment of the ^{129}Xe atom,” *Phys. Rev. A* **100**, 022505 (2019).
- [53] T. W. Kornack and M. V. Romalis, “Dynamics of two overlapping spin ensembles interacting by spin exchange,” *Phys. Rev. Lett.* **89**, 253002 (2002).
- [54] T. W. Kornack, R. K. Ghosh, and M. V. Romalis, “Nuclear spin gyroscope based on an atomic comagnetometer,” *Phys. Rev. Lett.* **95**, 230801 (2005).
- [55] J. Lee, A. Almasi, and M. Romalis, “Improved limits on spin-mass interactions,” *Phys. Rev. Lett.* **120**, 161801 (2018).

- [56] A. Almasi, J. Lee, H. Winarto, M. Smiciklas, and M. V. Romalis, “New limits on anomalous spin-spin interactions,” *Phys. Rev. Lett.* **125**, 201802 (2020).
- [57] M. Smiciklas, J. M. Brown, L. W. Cheuk, S. J. Smullin, and M. V. Romalis, “New Test of Local Lorentz Invariance Using a ^{21}Ne -Rb-K Comagnetometer,” *Physical Review Letters* **107**, 171604 (2011), [arXiv:1106.0738 \[physics.atom-ph\]](#) .
- [58] P. W. Graham, D. E. Kaplan, J. Mardon, S. Rajendran, h. Terrano, L. Trahms, and T. Wilkason, “Spin precession experiments for light axionic dark matter,” *Phys. Rev. D* **97**, 055006 (2018).
- [59] I. M. Bloch, Y. Hochberg, E. Kuflik, and T. Volansky, “Axion-like relics: new constraints from old comagnetometer data,” *Journal of High Energy Physics* **2020**, 167 (2020).
- [60] E. M. Purcell and N. F. Ramsey, “On the possibility of electric dipole moments for elementary particles and nuclei,” *Phys. Rev.* **78**, 807–807 (1950).
- [61] G. 't Hooft, “Symmetry breaking through bell-jackiw anomalies,” *Phys. Rev. Lett.* **37**, 8–11 (1976).
- [62] A. D. Sakharov, “Violation of cp invariance, ? asymmetry, and baryon asymmetry of the universe,” *Sov. Phys. JETP Lett.* **5**, 24 (1967).
- [63] T. G. Vold, F. J. Raab, B. Heckel, and E. N. Fortson, “Search for a permanent electric dipole moment on the ^{129}Xe atom,” *Phys. Rev. Lett.* **52**, 2229–2232 (1984).
- [64] N. Yamanaka, B. K. Sahoo, N. Yoshinaga, T. Sato, K. Asahi, and B. P. Das, “Probing exotic phenomena at the interface of nuclear and particle physics with the electric dipole moments of diamagnetic atoms: A unique window to hadronic and semi-leptonic CP violation,” *European Physical Journal A* **53**, 54 (2017), [arXiv:1703.01570 \[hep-ph\]](#) .
- [65] R. H. Parker, M. R. Dietrich, M. R. Kalita, N. D. Lemke, K. G. Bailey, M. Bishof, J. P. Greene, R. J. Holt, W. Korsch, Z.-T. Lu, P. Mueller, T. P. O’Connor, and J. T. Singh, “First measurement of the atomic electric dipole moment of ^{225}Ra ,” *Phys. Rev. Lett.* **114**, 233002 (2015).
- [66] M. Bishof, R. H. Parker, K. G. Bailey, J. P. Greene, R. J. Holt, M. R. Kalita, W. Korsch, N. D. Lemke, Z.-T. Lu, P. Mueller, T. P. O’Connor, J. T. Singh, and M. R. Dietrich, “Improved limit on the ^{225}Ra electric dipole moment,” *Phys. Rev. C* **94**, 025501 (2016).
- [67] T. Chupp and M. Ramsey-Musolf, “Electric dipole moments: A global analysis,” *Phys. Rev. C* **91**, 035502 (2015).
- [68] L. I. Schiff, “Measurability of nuclear electric dipole moments,” *Phys. Rev.* **132**, 2194–2200 (1963).
- [69] V. V. Flambaum and J. S. M. Ginges, “Nuclear schiff moment and time-invariance violation in atoms,” *Phys. Rev. A* **65**, 032113 (2002).
- [70] K. Yanase and N. Shimizu, “Large-scale shell-model calculations of nuclear schiff moments of ^{129}Xe and ^{199}Hg ,” *Phys. Rev. C* **102**, 065502 (2020).
- [71] T. Fleig and M. Jung, “ \mathcal{P} , \mathcal{T} -odd interactions in atomic ^{129}Xe and phenomenological applications,” *Phys. Rev. A* **103**, 012807 (2021).
- [72] G. Cocconi and E. Salpeter, “A search for anisotropy of inertia,” *Il Nuovo Cimento (1955-1965)* **10**, 646–651 (1958).
- [73] A. P. Lightman and D. L. Lee, “Restricted proof that the weak equivalence principle implies the einstein equivalence principle,” *Phys. Rev. D* **8**, 364–376 (1973).
- [74] S. Coleman and S. L. Glashow, “Cosmic ray and neutrino tests of special relativity,” *Physics Letters B* **405**, 249–252 (1997).
- [75] D. Colladay and V. A. Kostelecký, “CPT violation and the standard model,” *Phys. Rev. D* **55**, 6760–6774 (1997).
- [76] V. A. Kostelecký and C. D. Lane, “Constraints on lorentz violation from clock-comparison experiments,” *Phys. Rev. D* **60**, 116010 (1999).

- [77] O. W. Greenberg, “*cpt* violation implies violation of lorentz invariance,” *Phys. Rev. Lett.* **89**, 231602 (2002).
- [78] N. Arkani-Hamed, H.-C. Cheng, M. Luty, and J. Thaler, “Universal dynamics of spontaneous lorentz violation and a new spin-dependent inverse-square law force,” *Journal of High Energy Physics* **2005**, 029–029 (2005).
- [79] M. P. Haugan, “Energy conservation and the principle of equivalence,” *Annals of Physics* **118**, 156–186 (1979).
- [80] V. V. Flambaum and M. V. Romalis, “Limits on lorentz invariance violation from coulomb interactions in nuclei and atoms,” *Phys. Rev. Lett.* **118**, 142501 (2017).
- [81] H. Müller, S. Herrmann, C. Braxmaier, S. Schiller, and A. Peters, “Modern michelson-morley experiment using cryogenic optical resonators,” *Phys. Rev. Lett.* **91**, 020401 (2003).
- [82] C. Eisele, A. Y. Nevsky, and S. Schiller, “Laboratory test of the isotropy of light propagation at the 10^{-17} level,” *Phys. Rev. Lett.* **103**, 090401 (2009).
- [83] M. A. Hohensee, N. Leefer, D. Budker, C. Harabati, V. A. Dzuba, and V. V. Flambaum, “Limits on Violations of Lorentz Symmetry and the Einstein Equivalence Principle using Radio-Frequency Spectroscopy of Atomic Dysprosium,” *Physical Review Letters* **111**, 050401 (2013).
- [84] T. Pruttivarasin, M. Ramm, S. G. Porsev, I. I. Tupitsyn, M. S. Safronova, M. A. Hohensee, and H. Häffner, “Michelson-Morley analogue for electrons using trapped ions to test Lorentz symmetry,” *Nature* **517**, 592–595 (2015), [arXiv:1412.2194 \[quant-ph\]](#) .
- [85] C. Sanner, N. Huntemann, R. Lange, C. Tamm, E. Peik, M. S. Safronova, and S. G. Porsev, “Optical clock comparison for Lorentz symmetry testing,” *Nature* **567**, 204–208 (2019), [arXiv:1809.10742 \[physics.atom-ph\]](#) .
- [86] M. V. Romalis, D. Sheng, B. Saam, and T. G. Walker, “Comment on “new limit on lorentz-invariance- and *cpt*-violating neutron spin interactions using a free-spin-precession ^3He - ^{129}Xe comagnetometer”,” *Phys. Rev. Lett.* **113**, 188901 (2014).
- [87] F. Allmendinger, U. Schmidt, W. Heil, S. Karpuk, A. Scharth, Y. Sobolev, and K. Tullney, “Allmendinger et al. reply:,” *Phys. Rev. Lett.* **113**, 188902 (2014).
- [88] W. A. Terrano, J. Meinel, N. Sachdeva, T. E. Chupp, S. Degenkolb, P. Fierlinger, F. Kuchler, and J. T. Singh, “Frequency shifts in noble-gas comagnetometers,” *Phys. Rev. A* **100**, 012502 (2019).
- [89] J. E. Moody and F. Wilczek, “New macroscopic forces?” *Phys. Rev. D* **30**, 130–138 (1984).
- [90] B. A. Young, “Search for a gravity shift in the proton larmor frequency,” *Phys. Rev. Lett.* **22**, 1445–1446 (1969).
- [91] D. J. Wineland, J. J. Bollinger, D. J. Heinzen, W. M. Itano, and M. G. Raizen, “Search for anomalous spin-dependent forces using stored-ion spectroscopy,” *Phys. Rev. Lett.* **67**, 1735–1738 (1991).
- [92] B. A. Dobrescu and I. Mocioiu, “Spin-dependent macroscopic forces from new particle exchange,” *Journal of High Energy Physics* **2006**, 005–005 (2006).
- [93] P. Fadeev, Y. V. Stadnik, F. Ficek, M. G. Kozlov, V. V. Flambaum, and D. Budker, “Revisiting spin-dependent forces mediated by new bosons: Potentials in the coordinate-space representation for macroscopic- and atomic-scale experiments,” *Phys. Rev. A* **99**, 022113 (2019).
- [94] P. Vorob’ev and I. Kolokolov, “DETECTORS FOR THE COSMIC AXIONIC WIND,” *arXiv e-prints* , astro-ph/9501042 (1995), [arXiv:astro-ph/9501042 \[astro-ph\]](#) .
- [95] P. W. Graham and S. Rajendran, “New observables for direct detection of axion dark matter,” *Phys. Rev. D* **88**, 035023 (2013).
- [96] J. Hong, J. E. Kim, and P. Sikivie, “Nuclear dipole radiation from $\bar{\theta}$ oscillations,” *Phys. Rev. D* **42**, 1847–1850 (1990).

- [97] K. Blum, R. T. D’Agnolo, M. Lisanti, and B. R. Safdi, “Constraining axion dark matter with big bang nucleosynthesis,” *Physics Letters B* **737**, 30–33 (2014).
- [98] R. Alonso, D. Blas, and P. Wolf, “Exploring the ultra-light to sub-MeV dark matter window with atomic clocks and co-magnetometers,” *Journal of High Energy Physics* **2019**, 69 (2019), [arXiv:1810.00889 \[hep-ph\]](https://arxiv.org/abs/1810.00889) .
- [99] C. Abel, N. J. Ayres, G. Ban, G. Bison, K. Bodek, V. Bondar, M. Daum, M. Fairbairn, V. V. Flambaum, P. Geltenbort, K. Green, W. C. Griffith, M. van der Grinten, Z. D. Grujic, P. G. Harris, N. Hild, P. Iaydjiev, S. N. Ivanov, M. Kasprzak, Y. Kermaidic, K. Kirch, H.-C. Koch, S. Komposch, P. A. Koss, A. Kozela, J. Krempel, B. Lauss, T. Lefort, Y. Lemièrre, D. J. E. Marsh, P. Mohanmurthy, A. Mtchedlishvili, M. Musgrave, F. M. Piegsa, G. Pignol, M. Rawlik, D. Rebreyend, D. Ries, S. Rocchia, D. Rozpik, P. Schmidt-Wellenburg, N. Severijns, D. Shiers, Y. V. Stadnik, A. Weis, E. Wursten, J. Zejma, and G. Zsigmond, “Search for axionlike dark matter through nuclear spin precession in electric and magnetic fields,” *Phys. Rev. X* **7**, 041034 (2017).
- [100] T. Wu, J. W. Blanchard, G. P. Centers, N. L. Figueroa, A. Garcon, P. W. Graham, D. F. J. Kimball, S. Rajendran, Y. V. Stadnik, A. O. Sushkov, A. Wickenbrock, and D. Budker, “Search for axionlike dark matter with a liquid-state nuclear spin comagnetometer,” *Phys. Rev. Lett.* **122**, 191302 (2019).
- [101] T. Braine, R. Cervantes, N. Crisosto, N. Du, S. Kimes, L. J. Rosenberg, G. Rybka, J. Yang, D. Bowering, A. S. Chou, R. Khatiwada, A. Sonnenschein, W. Wester, G. Carosi, N. Woollett, L. D. Duffy, R. Bradley, C. Boutan, M. Jones, B. H. LaRoque, N. S. Oblath, M. S. Taubman, J. Clarke, A. Dove, A. Eddins, S. R. O’Kelley, S. Nawaz, I. Siddiqi, N. Stevenson, A. Agrawal, A. V. Dixit, J. R. Gleason, S. Jois, P. Sikivie, J. A. Solomon, N. S. Sullivan, D. B. Tanner, E. Lentz, E. J. Daw, J. H. Buckley, P. M. Harrington, E. A. Henriksen, and K. W. Murch (ADMX Collaboration), “Extended search for the invisible axion with the axion dark matter experiment,” *Phys. Rev. Lett.* **124**, 101303 (2020).
- [102] B. M. Graner, *Reduced Limit on the Permanent Electric Dipole Moment of 199Hg*, Ph.D. thesis, University of Washington (2017).
- [103] S. F. Huelga, C. Macchiavello, T. Pellizzari, A. K. Ekert, M. B. Plenio, and J. I. Cirac, “Improvement of frequency standards with quantum entanglement,” *Phys. Rev. Lett.* **79**, 3865–3868 (1997).
- [104] M. E. Limes, N. Dural, M. V. Romalis, E. L. Foley, T. W. Kornack, A. Nelson, L. R. Grisham, and J. Vaara, “Dipolar and scalar ^3He – ^{129}Xe frequency shifts in stemless cells,” *Phys. Rev. A* **100**, 010501 (2019).
- [105] J. S. Waugh, L. M. Huber, and U. Haeberlen, “Approach to high-resolution nmr in solids,” *Phys. Rev. Lett.* **20**, 180–182 (1968).
- [106] K. U. Schreiber, T. Klügel, and G. E. Stedman, “Earth tide and tilt detection by a ring laser gyroscope,” *Journal of Geophysical Research: Solid Earth* **108** (2003), <https://doi.org/10.1029/2001JB000569>, <https://agupubs.onlinelibrary.wiley.com/doi/pdf/10.1029/2001JB000569> .
- [107] K. U. Schreiber, A. Velikoseltsev, M. Rothacher, T. Klügel, G. E. Stedman, and D. L. Wiltshire, “Direct measurement of diurnal polar motion by ring laser gyroscopes,” *Journal of Geophysical Research: Solid Earth* **109** (2004), <https://doi.org/10.1029/2003JB002803>, <https://agupubs.onlinelibrary.wiley.com/doi/pdf/10.1029/2003JB002803> .
- [108] K. U. Schreiber and J. R. Wells, “Invited review article: Large ring lasers for rotation sensing,” *Review of Scientific Instruments* **84**, 041101 (2013), <https://doi.org/10.1063/1.4798216> .
- [109] <https://jewellinstruments.com/products/geo/ultra-precision/600-series/model-a603/>.
- [110] H. B. Dang, A. C. Maloof, and M. V. Romalis, “Ultrahigh sensitivity magnetic field and magnetization measurements with an atomic magnetometer,” *Applied Physics Letters* **97**, 151110 (2010), <https://doi.org/10.1063/1.3491215> .

- [111] D. Sheng, A. Kabcenell, and M. V. Romalis, “New classes of systematic effects in gas spin comagnetometers,” *Phys. Rev. Lett.* **113**, 163002 (2014).
- [112] A. Korver, D. Thrasher, M. Bulatowicz, and T. G. Walker, “Synchronous spin-exchange optical pumping,” *Phys. Rev. Lett.* **115**, 253001 (2015).
- [113] D. A. Thrasher, S. S. Sorensen, J. Weber, M. Bulatowicz, A. Korver, M. Larsen, and T. G. Walker, “Continuous comagnetometry using transversely polarized xe isotopes,” *Phys. Rev. A* **100**, 061403 (2019).
- [114] S. S. Sorensen, D. A. Thrasher, and T. G. Walker, “A synchronous spin-exchange optically pumped nmr-gyroscope,” *Applied Sciences* **10** (2020), 10.3390/app10207099.
- [115] T. Sato, Y. Ichikawa, S. Kojima, C. Funayama, S. Tanaka, T. Inoue, A. Uchiyama, A. Gladkov, A. Takamine, Y. Sakamoto, Y. Ohtomo, C. Hirao, M. Chikamori, E. Hikota, T. Suzuki, M. Tsuchiya, T. Furukawa, A. Yoshimi, C. Bidinosti, T. Ino, H. Ueno, Y. Matsuo, T. Fukuyama, N. Yoshinaga, Y. Sakemi, and K. Asahi, “Development of co-located 129xe and 131xe nuclear spin masers with external feedback scheme,” *Physics Letters A* **382**, 588–594 (2018).
- [116] T. Wu, J. W. Blanchard, D. F. Jackson Kimball, M. Jiang, and D. Budker, “Nuclear-spin comagnetometer based on a liquid of identical molecules,” *Phys. Rev. Lett.* **121**, 023202 (2018).
- [117] M. Pospelov, S. Pustelny, M. P. Ledbetter, D. F. J. Kimball, W. Gawlik, and D. Budker, “Detecting domain walls of axionlike models using terrestrial experiments,” *Phys. Rev. Lett.* **110**, 021803 (2013).
- [118] S. Afach, B. C. Buchler, D. Budker, C. Dailey, A. Derevianko, V. Dumont, N. L. Figueroa, I. Gerhardt, Z. D. Gruji?, H. Guo, C. Hao, P. S. Hamilton, M. Hedges, D. F. J. Kimball, D. Kim, S. Khamis, T. Kornack, V. Lebedev, Z.-T. Lu, H. Masia-Roig, M. Monroy, M. Padniuk, C. A. Palm, S. Y. Park, K. V. Paul, A. Penafior, X. Peng, M. Pospelov, R. Preston, S. Pustelny, T. Scholtes, P. C. Segura, Y. K. Semertzidis, D. Sheng, Y. C. Shin, J. A. Smiga, J. E. Stalnaker, I. Sulai, D. Tandon, T. Wang, A. Weis, A. Wickenbrock, T. Wilson, T. Wu, D. Wurm, W. Xiao, Y. Yang, D. Yu, and J. Zhang, “Search for topological defect dark matter using the global network of optical magnetometers for exotic physics searches (gnome),” (2021), [arXiv:2102.13379](https://arxiv.org/abs/2102.13379) [astro-ph.CO] .